Two-photon excitation of the lowest $4f^2 \rightarrow 4f5d$ near-ultraviolet transitions in $Pr^{3+}:Y_3Al_5O_{12}$

S. K. Gayen, Bin Qing Xie, and Y. M. Cheung
Department of Physics and Engineering Physics, Stevens Institute of Technology, Hoboken, New Jersey 07030
(Received 19 August 1991)

Two-photon transitions from the $^3H_4$ ground-state manifold of the $4f^2$ configuration to the lowest state of the $4f5d$ configuration of Pr^{3+} in $Y_3Al_5O_{12}$ have been studied with a tunable dye laser as a function of the excitation wavelength, intensity, temperature, and focusing geometry. The two-photon excitation spectrum is vibronic in nature and covers the 555–615-nm excitation wavelength range. Both the direct nonresonant and the resonantly enhanced transitions are observed. The measured two-photon-absorption cross section varies over 3 orders of magnitude with a maximum of 1×10^{-51} cm^{4}s at the peak of the resonantly enhanced transition at 581 nm. The parity selection rule which forbids these two-photon transitions in a free ion is relaxed by odd-parity crystal-field mixing of the wave functions, making these transitions possible. Two-photon excitation measurements are complemented by one-photon-absorption and -emission measurements.

I. INTRODUCTION

This paper presents the results of a study of first-order parity-forbidden $4f^2 \rightarrow 4f5d$ transitions in trivalent praseodymium (Pr^{3+}) ion doped yttrium aluminum garnet ($Y_3Al_5O_{12}$), commonly abbreviated as YAG. The Pr^{3+} ion has played a very important role in our understanding of optical and spectroscopic properties of impurity ion-activated insulators. The optical and spectroscopic properties of this ion both in the free-ion state as well as in many different crystalline and glassy hosts are well documented. A number of novel high-resolution and nonlinear laser spectroscopic studies on this ion doped in various crystals have been reported over the years. These include fluorescence line narrowing, four-wave mixing, photon echo, two-photon absorption (TPA), and polarization spectroscopy.[1] Laser action in a number of crystals doped with this ion has also been demonstrated.[2]

However, most of these studies have concentrated on transitions between Stark manifolds belonging to the same $4f^2$ electronic configuration which give rise to sharp lines in absorption and emission spectra. There is a paucity of detailed studies of the interconfigurational $4f^2 \rightarrow 4f5d$ transitions in this ion. One major reason for this scarcity is that, in most crystals, the $4f5d$ levels of Pr^{3+} ions are located at energies $\sim 50\,000$ cm^{-1} above the ground state.[3] So, these levels are not so readily accessible to conventional light sources. The strong ultraviolet (uv) absorption of the host lattice has limited the study of these transitions as well. In a pioneering study, Elias *et al.* used the intense uv radiation from a synchrotron-storage-ring source to conduct a study of the broadband linear absorption and emission spectra of Pr^{3+} in LaF_3 following excitation of the $5d$ and $6s$ states of the ion.[4] However, the energy-level structure of Pr^{3+} is different in YAG. The large crystal-field splitting of the $5d$ states in this crystal results in relatively low-lying $5d$ levels as compared to those in common hosts like LaF_3, CaF_2, etc.[5] However, the system has received only limited attention,[5–7] and a detailed study of its spectroscopic and quantum electronic properties yet remains to be completed. Hooge measured the one-photon absorption and fluorescence spectra involving $f \rightarrow f$ transitions between 16 K and room temperature.[6] Gourley completed a detailed analysis of the spectral linewidth of the $^3H_4 \rightarrow {}^3P_0$ transition in this crystal.[7] The study of the $5d$ states of Pr^{3+} in this crystal was undertaken by Weber, who investigated the radiative and nonradiative deexcitation of $5d$ states using the temperature dependence of fluorescence lifetime.[5]

Although the first experimental demonstration[8] of two-photon (TP) excitation involved the electronic $4f \rightarrow 5d$ transition in $Eu^{2+}:CaF_2$, the subsequent studies of two-photon transitions in rare-earth ion-doped crystals mostly centered on the sharp, parity-allowed $f \rightarrow f$ transitions in these ions. The theory of TP processes for these transitions is now well developed and provides quantitative agreement with experimental data.[9–11] Gayen *et al.*[12–14] carried out a detailed study of first-order parity-forbidden $4f \rightarrow 5d$ TP transitions in $Ce^{3+}:CaF_2$. Their theoretical interpretation[14] of the electronic zero-phonon transition has been further extended and provides reasonable qualitative agreement with experimental values of cross section and polarization anisotropy.[15,16] Two-photon absorption has been studied in Pr^{3+}-doped crystals as well.[17–19] All three reported studies have centered on the $^1S_0$ state, which happens to be the highest excited state in the $4f^2$ manifold of Pr^{3+} in the crystals investigated. Yen *et al.*[17] excited the state in LaF_3 by first populating the intermediate D levels by one-photon absorption, followed by a TP transition to the $^1S_0$ level. Bloembergen and co-workers studied the same level both in LaF_3 and $LaCl_3$ by a direct two-photon transition from the ground state.[18,19]

The thrust of the present study is to further extend and complement the current state of spectroscopic characteri-

zation of Pr^{3+}:YAG in two respects. First, it undertakes an investigation of the spectroscopic properties of Pr^{3+} ion in YAG, with particular emphasis on the lowest $5d$ state. Only a few studies on the $5d$ states of Pr^{3+} exist,[4,5] and even a detailed study of the states of $4f^2$ manifold of this ion in YAG is lacking. YAG has been proven to be an efficient host material which supports laser action in a number of ions doped into it. In this respect, the present work is expected to have practical implications. Second, it investigates two-photon transitions which are parity forbidden in the free ion, but acquire strength because of mixing of states of opposite parity by the odd-parity crystal field.

The observed room-temperature TP excitation spectra is a broad vibronic band which extends over the 555–615-nm spectral range. This spectral range corresponds, in two-photon absorption, to the range covered by the intense parity-allowed lowest $4f \rightarrow 5d$ one-photon absorption (OPA) spectrum. A very interesting feature of the TP spectrum is that, in addition to direct two-photon absorption transitions involving off-resonance intermediate states, resonantly enhanced TP transitions with about 2 orders of magnitude higher transition strength are observed. Since, the TP absorption cross sections are prohibitively small for direct absorption measurements, the near-uv Pr^{3+} fluorescence from the lowest $5d$ state was monitored as a function of excitation wavelength to achieve adequate sensitivity in detecting TP transitions. The energy gap between the lowest $5d$ level and the nearest $4f$ excited level being greater than 10 000 cm^{-1}, the quantum efficiency for $5d$ fluorescence is high.[5] In addition, most of the emission is over a limited spectral range far removed from the excitation wavelength range. These facts helped optimize the detection sensitivity for weak TP signal.

In Sec. II, we briefly present the results of our linear spectroscopic measurements on Pr^{3+}:YAG, which complement, and help analyze, the two-photon excitation measurements. Section III outlines the experimental procedure and parameters for two-photon excitation measurements, and Sec. IV presents experimental results. In Sec. V, a simple theoretical argument based on second-order, time-dependent, quantum-mechanical perturbation theory is provided for a qualitative understanding of experimental results. The measured TP excitation cross sections are compared to those observed in other ions, and the implications of experimental results are discussed.

II. ONE-PHOTON SPECTROSCOPY OF Pr^{3+}:YAG

The characteristics of single-photon absorption and emission spectra of Pr^{3+}:YAG, which are necessary for the interpretation of the two-photon excitation measurements, are presented in this section. The single-crystal sample used in all the measurements reported here was grown by the Czochralski method at the Crystal Products Division of Union Carbide. It contains 0.4% of the Pr^{3+} ion, which is equivalent to a concentration of 5.5×10^{19} ions/cm^3. The crystal is a 10-mm-long cylinder with its axis collinear with the [111] crystallographic axis. The exciting radiation for all measurements was incident along this axis of the sample.

The room-temperature absorption spectra of the crystal, taken with a Perkin-Elmer Lambda-9 uv–visible–near-infrared spectrophotometer are displayed in Figs. 1(a)–1(c). The two intense, broad bands at wavelengths shorter than 325 nm, in Fig. 1(a), are due to strong, electric-dipole transitions from the $^3H_4$

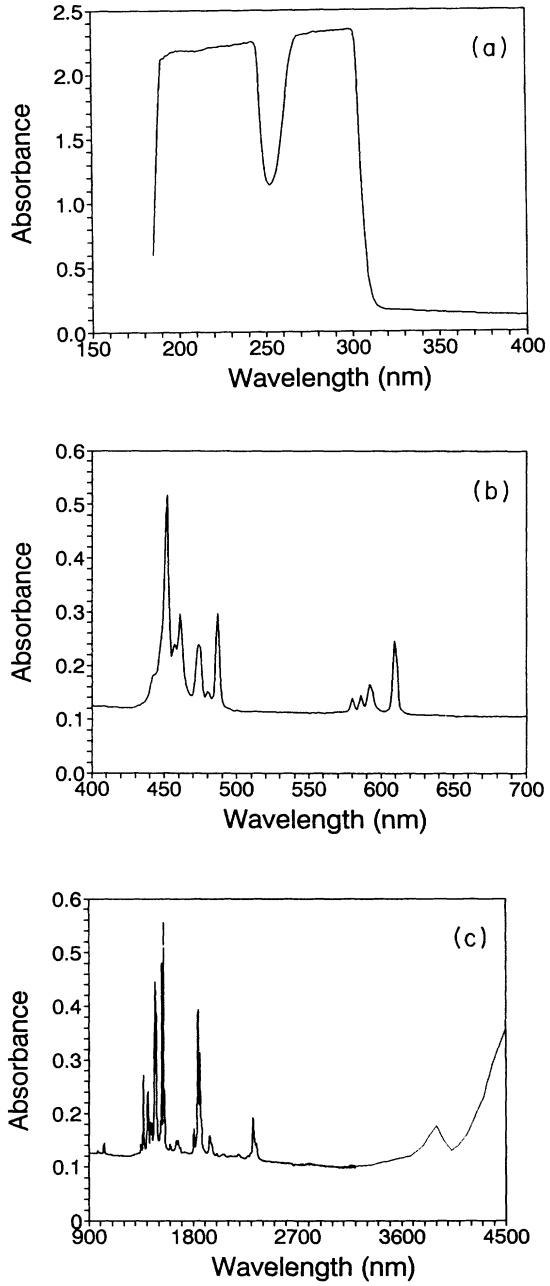

FIG. 1. One-photon absorption spectrum of 0.4% Pr^{3+}:$Y_3Al_5O_{12}$ at room temperature covering (a) 185–400-nm, (b) 400–700-nm, and (c) 900–4500-nm spectral regions. Spectrum beyond 3200 nm shown by dashed line in (c) was taken with an ir spectrometer as described in the text. No absorption was observed in the range 700–900 nm, so that spectral region is not displayed in the figure.

ground state of the $4f^2$ configuration to the two lower-lying states of the $4f5d$ configuration of the Pr^{3+} ion. Wavelengths shorter than 185 nm were not accessible to the spectophotometer. However, the onset of the fundamental absorption edge of YAG occurs around this wavelength, so measurements at shorter wavelengths may not reveal any distinct Pr^{3+} feature. The numerous sharp absorption lines below 450 nm are due to transitions from the $^3H_4$ ground state to the higher excited states of the $4f^2$ configuration. We have measured the infrared (ir) absorption spectrum of the sample down to 400 cm^{-1} (25 μm) using a Perkin-Elmer 983 infrared spectrometer. Part of that spectrum is combined with the spectrum taken with the uv–visible–near-ir spectrophotometer to generate the composite absorption spectrum shown in Fig. 1(c). The part of the spectrum taken with the ir spectrometer is shown by the dotted line. The additional feature revealed by the ir absorption measurement is the shallow structure centered at 3902 nm, and is attributed to absorptive transitions to the $^3H_5$ multiplet. At wavelengths longer than 4400 nm, the YAG host starts to absorb, so the spectrum is presented only up to 4500 nm showing the onset of host absorption. Thus of the 13 possible multiplets belonging to the $4f^2$ configuration, 12 are tentatively identified from the absorption measurements. The $^1S_0$ level, which lies $\sim$46 000 cm^{-1} above the ground state in other host materials,[17–19] and is expected to be about that far removed in this crystal, presumably overlaps with the second $5d$ level and may not be readily identified.

An energy-level diagram of Pr^{3+}:YAG constructed on the basis of our measurements is shown in Fig. 2. The extent of the boxed regions for the two $5d$ bands denotes the full width of the bands at one-half maximum. The solid circles indicate levels from which fluorescence was observed in our measurements which extended only up to 850 nm in the long-wavelength region. The positions of the multiplets of the $4f^2$ configuration are in agreement with previous experimental results.[5–7] The positions of $5d$ bands agree in general with Weber's measurement;[5] however, the second $5d$ band extends to higher energy in our sample than that reported in his work.

The room-temperature fluorescence spectrum of Pr^{3+}:YAG, over the 300–600-nm spectral range for excitation at 280 nm into the first $5d$ absorption band, is presented in Fig. 3. An exactly similar spectrum is obtained for excitation into the second $5d$ band at 240 nm. The fluorescence spectra were taken with a Perkin-Elmer Model LS-50 Luminescence Spectrometer. The strongest $5d$ fluorescence extends from 300 to 450 nm and is due to transitions terminating on the ^3F_J (J=2,3,4) and ^3H_J (J=4,5,6) manifolds. Although the estimated minimum $5d$-to-$4f$ energy gap is $\sim$10 000 cm^{-1}, and the lowest $5d$ state fluoresces with near-unity quantum efficiency,[5] weak nonradiative transitions from the lowest $5d$ state to the nearest $^3P_2$ manifold do indeed occur. Subsequent intraconfigurational nonradiative relaxation then populates the $^3P_0$ manifold. The radiative deexcitation of this manifold to the ground and the $^3H_5$ states results in the sharp, relatively weak fluorescence lines in the 480–570-nm spectral range. Even weaker emission at wavelengths

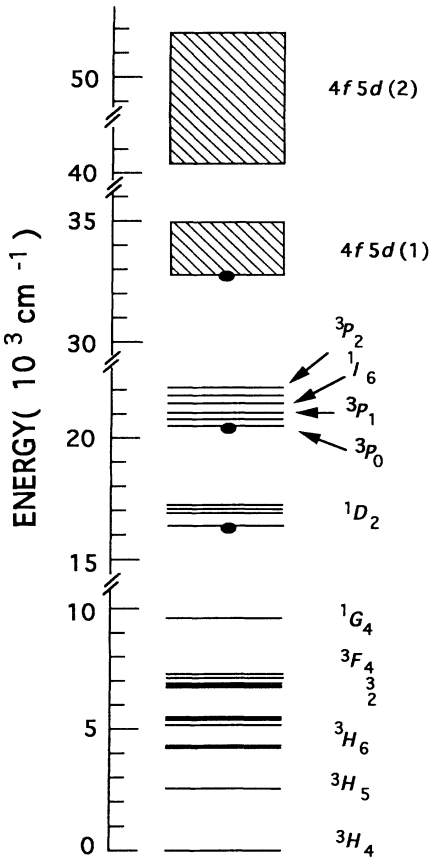

FIG. 2. An energy-level diagram for Pr^{3+} in YAG showing the locations of multiplets of $4f^2$ ground configuration and the first two lower states of the $4f5d$ excited configuration. Levels from which fluorescence has been observed are marked with solid ellipses.

between 610 and 750 nm has been observed (not displayed in the figure), which seems to include overlapping contributions from the lowest $5d \rightarrow {}^1D_2$ and ${}^1D_2 \rightarrow {}^3H_4, {}^3H_5$ transitions. This is inferred from multicomponent decay of fluorescence in this spectral region. However, the details of the fluorescence dynamics are not the thrust of this article and will be presented elsewhere.

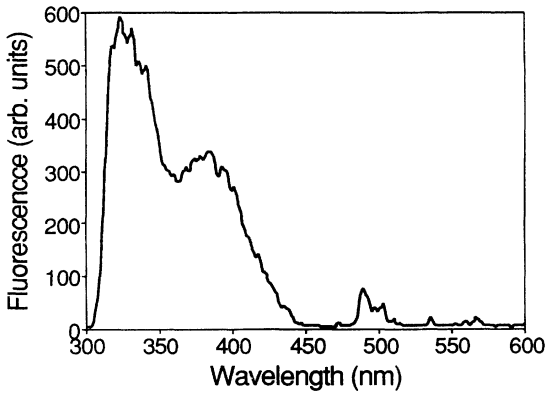

FIG. 3. A room-temperature fluorescence spectrum of Pr^{3+}:YAG for excitation at 280 nm into the lowest $4f5d$ absorption band.

For the two-photon excitation measurement we monitored the fluorescence in the 300–450-nm range. The fluorescence lifetime in this spectral region was measured following two-photon excitation of the lowest $5d$ state with 7-ns pulses from a dye laser. From a simple-exponential fit of the fluorescence decay, a room-temperature fluorescence lifetime of 25 ± 5 ns is estimated, which is in agreement with the previously published result.[5]

III. EXPERIMENTAL ARRANGEMENT

The experimental arrangement for two-photon excitation measurements is shown in Fig. 4. The two-photon transitions were excited by 7-ns pulses from a frequency-tunable dye laser pumped by the second harmonic of a Nd:YAG laser (Spectra Physics DCR-3G). The dye-laser consists of an oscillator and an amplifier. The oscillator uses a dual-prism beam expander and a 600-line/mm blazed grating in Littrow as the back mirror to produce narrow-bandwidth pulses. The dye laser may be continuously tuned by angle-tuning the diffraction grating. The output of the oscillator is further amplified by the amplifier stage as needed. The dye-laser output has a nominal bandwidth of $\sim 0.1\ \mathrm{cm}^{-1}$. The dye-laser beam is focused into the sample by a 1-m focal length lens. A small fraction of the dye-laser beam energy is sent to a monochromator for frequency calibration.

The sample used in this study has been described in Sec. II. The sample was mounted on a cold finger in the tail section of a cryostat, which uses a small pool of liquid nitrogen to cool the sample by conduction. The dye-laser beam is vertically polarized and is incident along the [111] axis of the crystal. The alignment of the sample axis with respect to the horizontal laser beam and a vertical reference direction was accurate to $\pm 2°$.

The $5d$ to ^3F_J and ^3H_J Pr^{3+} fluorescence was collected at right angles to the laser beam and collimated by a 5-cm-diameter, 10-cm-focal-length lens placed 10 cm away from the sample. The collimated light was converged by an identical second lens and passed through a set of visible-absorbing, uv-transmitting filters (two Corning 7-54, one 7-59, and a 4-80) before being detected by a photomultiplier tube with S-20 response. A silicon photodiode (Hamamatsu S-2386-18 K) calibrated against a laser-energy meter (Scientech Model 36-0001) was used to monitor the changes in the dye-laser pulse energy. Both the photodiode and the photomultiplier current outputs were integrated by collecting capacitors, which in parallel with a resistor, provide a voltage output with a 50-μs decay time. These signals were sensed by identical gated integrators and boxcar averagers (Stanford Research Systems Model SR250) and processed by an IBM AT compatible microcomputer.

Three different dyes (Exciton DCM+Rhodamine 610, Rhodamine 610+Rhodamine 590, and Rhodamine 590) dissolved in methanol were used to provide overlapping spectra in the 615–555-nm spectral region. The fluorescence signal was normalized by the square of the dye-laser pulse energy to account for the variations of the pulse energy. The normalized ratio was averaged over 100 laser pulses at each wavelength to achieve an adequate signal-to-noise ratio against the random fluctuations in the dye-laser pulse energy and temporal profile.

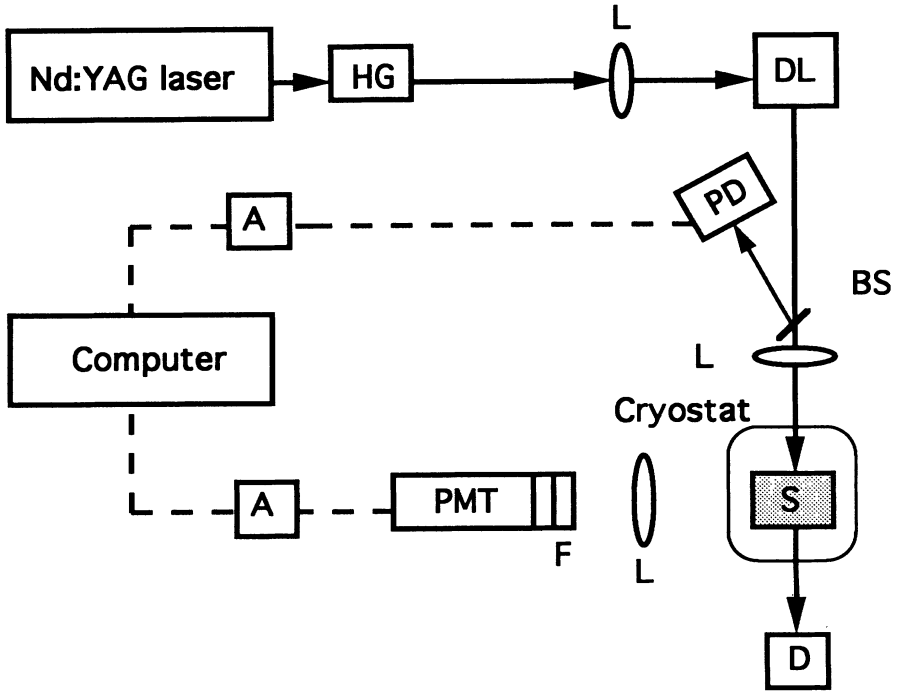

FIG. 4. A schematic diagram of the experimental arrangement used for two-photon excitation measurement. Key: A=gated integrator and boxcar averager, BS=beam splitter, D=beam dump, DL=dye laser, F=filter, HG=harmonic generator, L=lens, PD=photodiode, PMT=photomultiplier tube, S=sample.

IV. EXPERIMENTAL RESULTS

A. Two-photon excitation spectra

The two-photon excitation spectra at room and liquid-nitrogen temperatures are displayed in Fig. 5. The room-temperature spectrum is a broadband covering the 615–555-nm spectral range. The salient features of this spectrum are the strong resonance peaks centered at 610, 593, 587, and 581 nm. The two-photon signal at these resonance wavelengths are about 2 orders of magnitude higher than the signal observed at other wavelengths. In order to show the relative strengths of these transitions with other transitions, it was thus necessary to present the TP signal on a logarithmic scale. At liquid-nitrogen temperature, another narrow, sharp peak appears at 614.4 nm, in addition to those observed in the room-temperature spectrum. A significant decrease in the fluorescence intensity at wavelengths shorter than but close to 614.4 nm is observed in the low-temperature spectrum as compared to that in the room-temperature spectrum. In addition, the shorter-wavelength sideband exhibits more structure at low temperature, and the structures of the peaks become better resolved.

The sharp line at 614.4 nm is a zero-phonon line which arises from a direct two-photon absorption process causing a purely electronic transition from the $^3H_4$ ground state to the lowest $4f5d$ state. The broad and structured sideband at shorter wavelengths is the phonon sideband of this electronic transition, and originates in vibronic transitions between the two states. Like the zero-phonon line, the phonon sideband (except for the peaks mentioned above) is due to direct TP transitions between the initial and final states. These transitions involve only nonresonant intermediate states, no real intermediate state is physically occupied by the ions making the transitions.

However, each of the strong resonance peaks centered at 610, 593, 587, and 581 nm in the TP excitation spectrum corresponds to a one-photon absorption maxima in Fig. 1, or to a transmission minima as displayed in the one-photon transmission spectrum in Fig. 5 (the lower dashed curve). This indicates that the TP absorption process is resonantly enhanced when the excitation wavelength is resonant with a one-photon transition in the sample. The interpretation of the resonantly enhanced and nonresonant TP transitions will be discussed further in a latter section.

In order to verify the two-photon nature of the excitation process, we have measured the dye-laser power dependence of the fluorescence strength. A set of calibrated neutral density filters was used in the dye-laser beam to attenuate the power as desired, thus avoiding the systematic error which may result from controlling the dye-laser power by varying the YAG-laser lamp energy. Figure 6 displays the results of the measurements done both for a resonantly enhanced transition for excitation at 581 nm, as well as for a nonresonant TP transition at

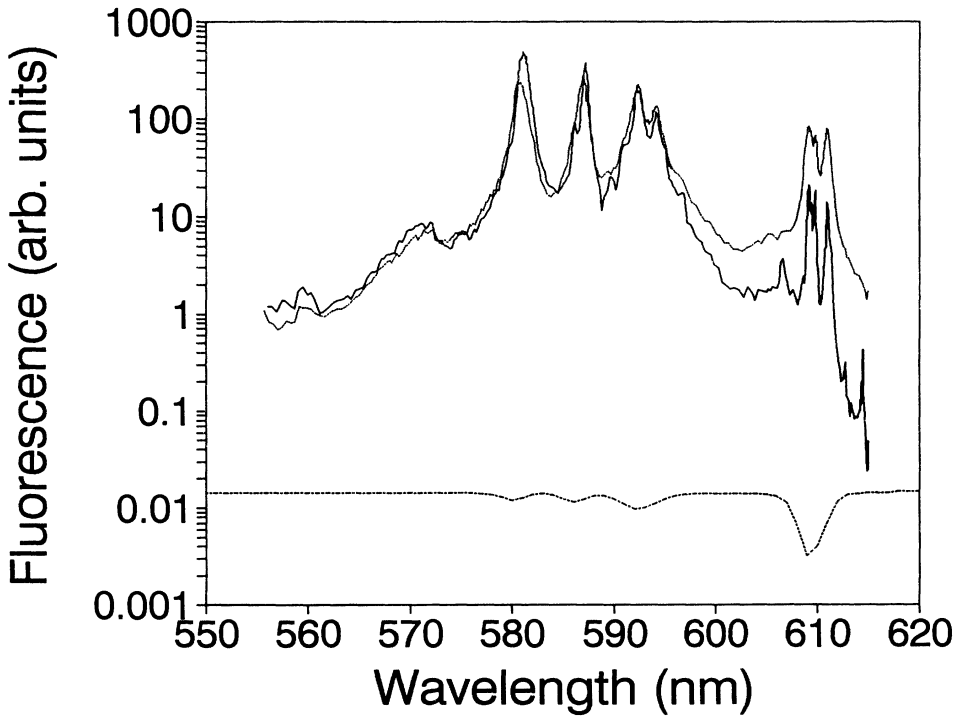

FIG. 5. Composite two-photon excitation spectra of 0.4% Pr^{3+}:YAG: (a) at liquid-nitrogen temperature (solid, heavier line), and (b) at room temperature (dotted, lighter line). The fluorescence intensity has been point by point normalized to the square of the dye-laser power. The lower dashed curve shows the positions of one-photon (OP) transmission minima of the sample over the same wavelength range as that in the TP spectra. The baseline of the OP transmission curve has been arbitrarily shifted to make the transmission minima more prominent. The OP transmission curve is not drawn to the scale either.

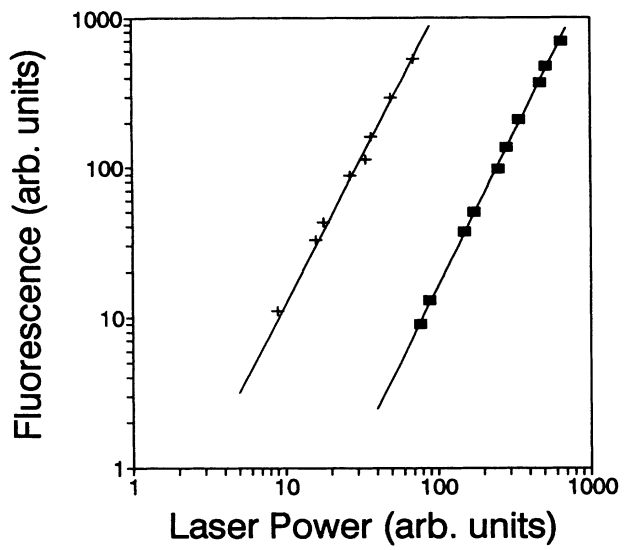

FIG. 6. Excitation power dependence of Pr^{3+} emission. Each point represents the average of five measurements, each of which has been averaged over 100 laser shots. The upper curve (crosses) is for excitation of a resonantly enhanced transition at 581 nm, the lower curve (solid squares) is for excitation of a nonresonant transition at 571 nm. The straight lines have a slope of 2.

571 nm. A quadratic dependence of the fluorescence strength on the dye-laser power is observed as expected for a two-photon absorption process. We have observed similar quadratic dependences for other resonantly enhanced transitions, and direct TP transitions for excitation at other wavelengths as well.

B. Measurement of two-photon absorption cross section

We have made an approximate measurement of the cross section for two-photon absorption for excitation at the vacuum wavelength of 581 nm, which corresponds to the peak of one of the resonantly enhanced transitions in the excitation spectrum of Fig. 5. Following the common practice in the literature, the TPA cross section σ is defined such that the induced transition rate per ion, W, is given by

$$W=\sigma F^2 , \tag{1}$$

where F is the incident photon flux in units of photons/cm^2 s, and σ is in cm^4 s. If ρ is the Pr^{3+} density in ions/cm^3, then the number of ions excited per laser pulse of duration T is[12]

$$N=T\rho\sigma\int_{-L/2}^{L/2}\int_0^R F^2(r,z)2\pi r\,dr\,dz , \tag{2}$$

where L and R are length and radius of the sample, respectively. The spatial profile of the dye-laser beam was scanned by a narrow slit and the flux distribution was found to be approximated by a Gaussian

$$F(r,z)=(2P/\pi w^2)\exp(-2r^2/w^2) , \tag{3}$$

where P is in photons/s, and w is the beam radius that varies with the propagation distance z. The focusing characteristics of the beam were found to be well approximated by

$$w^2(z)=w_0^2\{1+[2(z-z_0)/b]^2\} , \tag{4}$$

where the minimum beam radius w_0 is at $z=z_0$, and $b=2\pi w_0^2/\lambda$ is the confocal parameter. Since the sample radius is very large compared to the dye-laser beam radius at the sample, the upper limit on the radial integral in Eq. (2) may be set to ∞. Using the descriptions of $F(r,z)$ and $w(z)$ given by Eqs. (3) and (4), the integral in Eq. (2) may then be expressed in a closed form as[12]

$$N=\frac{T\rho\sigma P^2}{\lambda}\{\tan^{-1}[(L-2z_0)/b] + \tan^{-1}[(L+2z_0)/b]\} . \tag{5}$$

The dependence of N on z_0 may be used to obtain an effective minimum waist w_0, and to determine the geometry for the optimal two-photon signal. Using the geometry of Fig. 7, z_0 can be related to the sample-to-lens separation x, and the lens-to-minimum-waist distance d_2. In the far field of the dye laser, the value of d_2 is nearly independent of d_1, and one may vary z_0 by moving the lens instead of the sample.[20] The result of measurement of Pr^{3+} fluorescence as a function of z_0 is shown in Fig. 8. The solid line represents a fit of the experimental data denoted by solid squares to the bracketed term in Eq. (5) for $b=14.3$ cm. This leads to an effective beam waist parameter of 114.9 μm, which agrees well with a 113-μm value estimated from scanning a 10-μm slit across the focal point. For our 1-cm-long sample $L/b\sim 0.07$, which implies that the excitation intensity does not vary too much over the pumped volume of the sample. This loose focusing geometry also reduces the possibility of unwanted Stark mixing, as well as surface and bulk damage of the sample, while providing an adequate signal for measurement.

In our measurements, the minimum waist is located at the center of the sample ($z_0=0$), and Eq. (5) takes the simpler form

$$N=\frac{2T\rho\sigma P^2}{\lambda}\tan^{-1}(L/b) . \tag{6}$$

The number of ions, N excited by a laser pulse may be es-

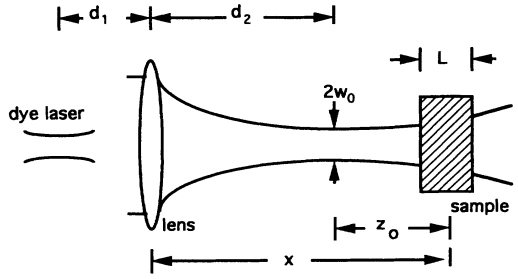

FIG. 7. Focusing geometry for two-photon excitation measurement and determination of the effective waist w_0. The dye-laser to focusing-lens separation is 400 cm.

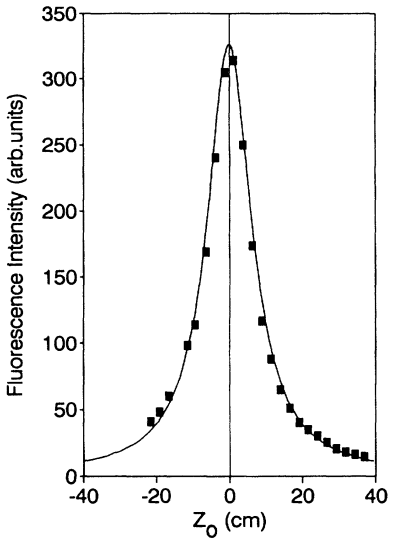

FIG. 8. Dependence of the fluorescence signal on the sample-to-waist separation, w_0. The solid line is a fit to the experimental data represented by solid squares using the bracketed term in Eq. (5) for $b=14.3$ cm, which yields $w_0=114.9$ μm.

timated from the peak voltage V per pulse measured across the integrating capacitor at the photomultiplier anode,[12]

$$V=QN(\Delta\Omega/4\pi)(\alpha q v)\ , \tag{7}$$

where Q, the fluorescence quantum efficiency, is taken to be unity,[5] the geometrical collection efficiency $\Delta\Omega/4\pi$ is 0.007, q is the quantum efficiency of the photomultiplier cathode, v is the voltage per photoelectron from the photocathode, and α represents the losses at the air-glass interfaces and through the optical filters in the collection path. We have estimated a value of 3.1×10^{-8} V/photon for the factor $\alpha q v$ by carefully calibrating the photomultiplier tube and collection-optics response to a well-characterized laser-light pulse. The dye-laser energy for this cross-section measurement was maintained at about 0.26 mJ per pulse, which is equivalent to 1.08×10^{23} photons/s. The resulting intensity at the sample is 89.6 MW/cm^2. At the peak of the resonantly enhanced TP transition at 581 nm, the peak voltage across the integrating capacitor was measured to be 2.2 V. Using these parameters with Eqs. (6) and (7), the peak cross section is estimated to be 1×10^{-51} cm^{4}s. Similar measurements yield a value of 4×10^{-53} cm^{4}s for nonresonant TP cross section at the phonon sideband at 578 nm, and 8×10^{-55} cm^{4}s for the zero-phonon transition at 614.4 nm. Values of the TP cross section thus estimated are accurate to within a factor of 10 because of the uncertainties in the intensity of the dye-laser beam, variations in its spatial and temporal profiles, and above all the calibration of the photomultiplier tube.

V. DISCUSSION

The two-photon excitation spectrum of Pr^{3+}:YAG is characterized by two distinct types of transitions: first, the resonantly enhanced transitions involving real intermediate states; and second, the direct two-photon transitions involving nonresonant intermediate states. Two-photon transitions involving nonresonant intermediate states include a zero-phonon line corresponding to a purely electronic transition, and an associated phonon sideband which arises from vibronic transitions. The peak cross section for resonantly enhanced transitions is about 2 orders of magnitude larger than the peak cross section for direct, nonresonant transitions. The resonantly enhanced TP transitions may be looked upon as involving an $f\rightarrow f$ transition from the ground to the intermediate state, and an allowed electric-dipole transition from the intermediate $4f$ state to the final $5d$ state, but should not be confused with a two-step process. The one-photon $f\rightarrow f$ transitions in rare-earth ion-doped crystals are well explained by the Judd-Ofelt theory.[21,22] Thus the relative strength of the resonantly enhanced transitions may be understood. Similar resonance enhancement has been reported in three-photon absorption from the $^4I_{9/2}$ ground state to the states of the $4f^25d$ configuration in Nd^{3+}:YAG.[23]

A semiquantitative understanding of some of the experimental results involving resonantly enhanced transitions may be obtained in terms of a simple second-order perturbation-theoretical description of the two-photon absorption (TPA) process. According to this theory, the TPA cross section per photon per ion in the electric-dipole approximation, for the general case of impurity ions in solids, is given by[9,23–25]

$$\sigma=\frac{16\pi^4e^4}{h^2c^3}(\eta_1\eta_2)^2\frac{\nu_1\nu_2}{n_1n_2}L(\nu)\left|\sum_i\left[\frac{\langle f|\hat{\mathbf{e}}_1\cdot\mathbf{r}|i\rangle\langle i|\hat{\mathbf{e}}_2\cdot\mathbf{r}|g\rangle}{\nu_{ig}-\nu_2-i\gamma_i/2}+\frac{\langle f|\hat{\mathbf{e}}_2\cdot\mathbf{r}|i\rangle\langle i|\hat{\mathbf{e}}_1\cdot\mathbf{r}|g\rangle}{\nu_{ig}-\nu_1-i\gamma_i/2}\right]\right|^2, \tag{8}$$

where $|g\rangle$, $|i\rangle$, and $|f\rangle$ are the ground, intermediate, and final states of the transition, $L(\nu)$ is the normalized line-shape function, ν_{ig} is the ground-to-intermediate-state energy splitting in cm^{-1}, and γ_i is the full width at half maximum (FWHM) breadth in wave numbers of the energy level $|i\rangle$, which is assumed to have a Lorentzian probability distribution. The subscript k (=1,2) refers to the kth photon with a frequency ν_k in cm^{-1}, and a polarization unit vector $\hat{\mathbf{e}}_k$. The index of refraction at that frequency is n_k, and $\eta_k=(n_k^2+2)/3$ is the local-field correction.[26] Damping is introduced phenomenologically so that the denominators at resonance become equal to $i\gamma$'s.

The summation in Eq. (8) extends over all the intermediate states of the active ion, and even for a moderately complex ion the states are not well known, and direct evaluation of the sum is impractical. Sophisticated ap-

proximation schemes are necessary to evaluate the sum, and the adequacy of those schemes may be tested by comparing the predictions of the theory to the experimental results. However, Eq. (8) predicts a resonance in the TPA cross section if one of the exciting photons becomes resonant with an intermediate state, making a one-photon transition to that state possible, and if an energy-conserving final state located at an energy of $\nu_1+\nu_2$ cm^{-1} is available. An order-of-magnitude estimate of the size of the resonantly enhanced TPA cross section may be made by assuming that the resonant intermediate state is the only state that contributes appreciably to the cross section so that the sum is replaced by a single term. For a resonantly enhanced transition this is a reasonable approximation, since the energy denominator for the term involving the resonant state is much smaller than those involving other virtual intermediate states. The resonant term then makes the dominant contribution to the cross section. Under this assumption, and for our experimental condition which uses two identical photons to excite a transition, Eq. (8) reduces to

$$\sigma = \frac{64\pi^4\nu^2\eta^4}{n^2h^2c^3}\frac{|\mu_{fi}\mu_{ig}|^2}{\gamma^2}L(\nu)\ , \tag{9}$$

where μ_{km} is the electric-dipole matrix element connecting levels $|k\rangle$ and $|m\rangle$. Equation (9) may now be evaluated by assuming the following parameters to obtain an estimate of the cross section. The typical value of electric-dipole transition moments for intra-$4f$ transitions in trivalent rare-earth (R^{3+}) ions in a crystal field is $\sim 2\times 10^{-20}$ esu.[23] However, a close examination of the absorption spectrum in Fig. 1 reveals that the one-photon transition to the intermediate state is a very weak one and we estimate the transition moment to be $|\mu_{ig}| = 1\times 10^{-21}$ esu. The value of $|\mu_{fi}|$ is taken to be 1×10^{-18} esu, typical of $4f \rightarrow 5d$ interconfigurational transition moments. The line width (FWHM) of the intermediate state is 33 cm^{-1}; and $L(\nu) = W^{-1} = (5340\ \text{cm}^{-1})^{-1}$, where W is the FWHM of the first $5d$ band. The index of refraction of YAG is 1.82, and the photon energy, ν is 17 212 cm^{-1}. Substituting all these parameters in Eq. (9), the peak TPA cross section for the resonantly enhanced transition at 581 nm is found to be 3×10^{-51} cm^{4}s. Given the uncertainties in the experimental value of 1×10^{-51} cm^{4}s, the theoretical estimate is in reasonable agreement.

However, a direct two-photon transition from a $4f$ to a $5d$ state is parity forbidden to first order. The observed appearance of the zero-phonon line (ZPL) in the TP spectrum may be explained in terms of the crystal-field parity mixing among the states involved in the transition. The Pr^{3+} ion in YAG is at a site of D_{2d} point-group symmetry,[27] and the odd-parity component of the crystal field can mix the $5d$ states with the $^3H_4$ ground state, and $4f$ and presumably $6s$ states with the lowest-$5d$ final state. The parity selection rule is thus relaxed, making a TP transition between mixed-parity initial and final states possible. The measured peak two-photon cross section of 8×10^{-55} cm^{4}s for the zero-phonon transition is comparable to the 2×10^{-54} cm^{4}s value[12] for a similar transition in Ce^{3+}:CaF_2.

The phonon sideband owes its origin to two different contributions of comparable strength. First, because of the odd-parity crystal-field mixing of wave functions, the zero-phonon line and vibrational progressions built on it appear in the TP excitation spectrum. Second, phonon-assisted transitions induced by the vibronic coupling give rise to totally symmetric progressions built on false origins. The experimentally observed TP spectrum is a superposition of both the contributions. A similar situation was observed[12-14] in the TPE spectrum of Ce^{3+}:CaF_2.

Although a qualitative explanation of the observed direct TP transitions may thus be provided, a theoretical calculation of the TP cross section is more involved. The standard second-order perturbation theory of $4f \rightarrow 4f$ two-photon transitions in RE ions by Axe[9] has been proven to be inadequate in some cases.[28,29] Further expansion of this theory by Judd and Pooler[10] and Downer and Bivas[11] through the introduction of third- and fourth-order corrections to the initial, intermediate, and final wave functions have led to significant improvements. However, this theory is not applicable to $4f \rightarrow 5d$ transitions presented here. A theory for $4f \rightarrow 5d$ TP transitions has to start with third-order corrections involving crystal-field interaction which should have odd parity. Even-parity crystal-field (CF), and spin-orbit (s.o.) interactions may contribute to transition strength in fourth or even higher orders. Development of such a third-order theory for purely electronic TP transitions has been undertaken by Leavitt who considered both static and dynamic crystal-field contributions,[15] as well as by Makhanek *et al.* who considered only static CF effects.[16] A more comprehensive theory will require the incorporation of even higher-order corrections involving the CF and s.o. interactions, as well as ligand-dependent effects.[30] A detailed analysis of direct TP transitions in Pr^{3+}:YAG along this line will be presented in a forthcoming article.

The theoretical formalism used above to estimate the cross section for resonantly enhanced two-photon absorption treats the transition process as one involving the simultaneous absorption of two identical photons. This is indeed the case for a direct TP transition where no resonant intermediate state is involved. A similar situation generally follows for a near-resonant, or resonant process as well. The process is coherent and may be looked upon as the effect of one photon modulating the energy spectrum of the matter in such a way that the second may be absorbed within the duration of the modulation (T_2). However, for the case of a resonant intermediate state, the excitation process may involve linear absorption to a real intermediate level followed at a later time by the absorption of a second photon. Such a two-step process is incoherent, the lifetime of the stationary intermediate state (T_1) enters dominantly into the absorption cross section. Since $T_1 > T_2$, such a two-step process, in many cases, may be much stronger even than a resonantly enhanced TP transition.[31] In a two-step process, it is also possible for the system to undergo some nonradiative relaxation before the second photon completes the transi-

tion process. As pointed out by Singh and Geusic,[32] the measured fluorescence intensity may then depend on the duration of the excitation light pulse. However, in the lowest order the transition rate for both the processes will have a quadratic dependence on laser intensity with a cross section given by Eq. (8).[23]

VI. CONCLUSIONS

First-order parity-forbidden two-photon transitions from the $^3H_4$ ground manifold of the $4f$ state to the lowest $5d$ excited state in Pr^{3+}:YAG have been observed. The low-temperature spectrum is characterized by a sharp zero-phonon line at an excitation wavelength of 614.4 nm corresponding to a purely electronic transition between the initial and the final states. The zero-phonon line is accompanied by a structured phonon sideband. As the excitation wavelength is tuned to one-photon resonances, about 2–3 orders of magnitude enhancement in transition strength is observed. The peak cross section for the resonantly enhanced TP transition for the excitation wavelength of 581 nm is 1×10^{-51} cm^{4}s. An estimate of the TP cross section in terms of a second-order-perturbation theoretical model is in a reasonable agreement with the measured value. The TP cross section for the zero-phonon transition is 8×10^{-55} cm^{4}s, and has a comparable magnitude for the phonon sideband. Static and dynamic odd-parity crystal-field effects in third order, and even-parity crystal field and spin-orbit interactions in fourth or higher order, are expected to be responsible for the relaxation of the parity selection rule, making the observed transitions possible.

ACKNOWLEDGMENTS

The authors gratefully acknowledge Professor T. R. Hart for the loan of several pieces of equipment, as well as for his overall support, and Dr. Milan Kokta for providing the crystal used in this study.

[1]The literature dealing with the spectroscopic studies of praseodymium ion in different host crystals is rather extensive. For a representative sampling, see *Laser Spectroscopy of Solids,* edited by W. M. Yen and P. M. Selzer (Springer-Verlag, Berlin, 1981).

[2]For a listing of Pr^{3+}-doped crystals in which laser action has been demonstrated, see A. A. Kaminskii, *Laser Crystals,* 2nd ed. (Springer-Verlag, Berlin, 1990).

[3]G. H. Dieke, in *Spectra and Energy Levels of Rare Earth Ions in Crystals,* edited by H. M. Crosswhite and H. Crosswhite (Interscience, New York, 1968.)

[4]L. R. Elias, Wm. S. Heaps, and W. M. Yen, Phys. Rev. B **8**, 4989 (1973).

[5]M. J. Weber, Solid State Commun. **12**, 741 (1973).

[6]F. N. Hooge, J. Chem. Phys. **45**, 4504 (1966).

[7]J. T. Gourley, Phys. Rev. B **5**, 22 (1972).

[8]W. Kaiser and C. G. B. Garret, Phys. Rev. Lett. **7**, 229 (1961).

[9]J. D. Axe, Jr., Phys. Rev. A **136**, 42 (1964).

[10]B. R. Judd and D. R. Pooler, J. Phys. C **15**, 591 (1982).

[11]M. C. Downer and A. Bivas, Phys. Rev. B **28**, 3677 (1983).

[12]S. K. Gayen and D. S. Hamilton, Phys. Rev. B **28**, 3706 (1983).

[13]S. K. Gayen, G. J. Pogatshnik, and D. S. Hamilton, J. Lumin. **31/32**, 260 (1984).

[14]S. K. Gayen, D. S. Hamilton, and R. H. Bartram, Phys. Rev. B **34**, 7523 (1986).

[15]R. C. Leavitt, Phys. Rev. B **35**, 9271 (1987).

[16]A. G. Makhanek, V. S. Korolkov, and L. A. Yuguryan, Phys. Status Solidi B **149**, 231 (1988).

[17]W. M. Yen, C. G. Levey, S. Huang, and S. T. Lai, J. Lumin. **24/25**, 659 (1981).

[18]C. D. Cordero-Montalvo and N. Bloembergen, Phys. Rev. B **30**, 438 (1984).

[19]R. S. Rana, C. D. Cordero-Montalvo and N. Bloembergen, J. Chem. Phys. **81**, 2951 (1984).

[20]E. H. A. Granneman and M. J. van der Weil, Rev. Sci. Instrum. **46**, 332 (1975).

[21]B. R. Judd, Phys. Rev. **127**, 750 (1962).

[22]G. S. Ofelt, J. Chem. Phys. **37**, 511 (1962).

[23]M. A. Kramer and R. W. Boyd, Phys. Rev. B **23**, 986 (1981).

[24]B. Honig, J. Jortner, and A. Szoke, J. Chem. Phys. **46**, 2714 (1967).

[25]A. Gold and J. P. Hernandez, Phys. Rev. **139**, A2002 (1965).

[26]W. B. Fowler, in *Physics of Color Centers,* edited by W. B. Fowler (Academic, New York, 1968), p. 64.

[27]H. G. Danielmeyer, in *Lasers,* edited by A. K. Levine and A. J. DeMaria (Marcel Dekker, New York, 1976) Vol. 4, p. 5 and references therein.

[28]M. Dagenais, M. Downer, R. Neumann, and N. Bloembergen, Phys. Rev. Lett. **46**, 561 (1981).

[29]M. C. Downer, A. Bivas, and N. Bloembergen, Opt. Commun. **41**, 335 (1982).

[30]M. F. Reid and F. S. Richardson, Phys. Rev. B **29**, 2830 (1984).

[31]H. Mahr, in *Nonlinear Optics: A Treatise,* edited by H. Rabin and C. L. Tang (Academic, New York, 1975), Vol. 1, p. 311.

[32]S. Singh and J. E. Geusic, in *Optical Properties of Ions in Crystals,* edited by H. M. Crosswhite and H. W. Moos (Interscience, New York, 1967), pp. 493–505.

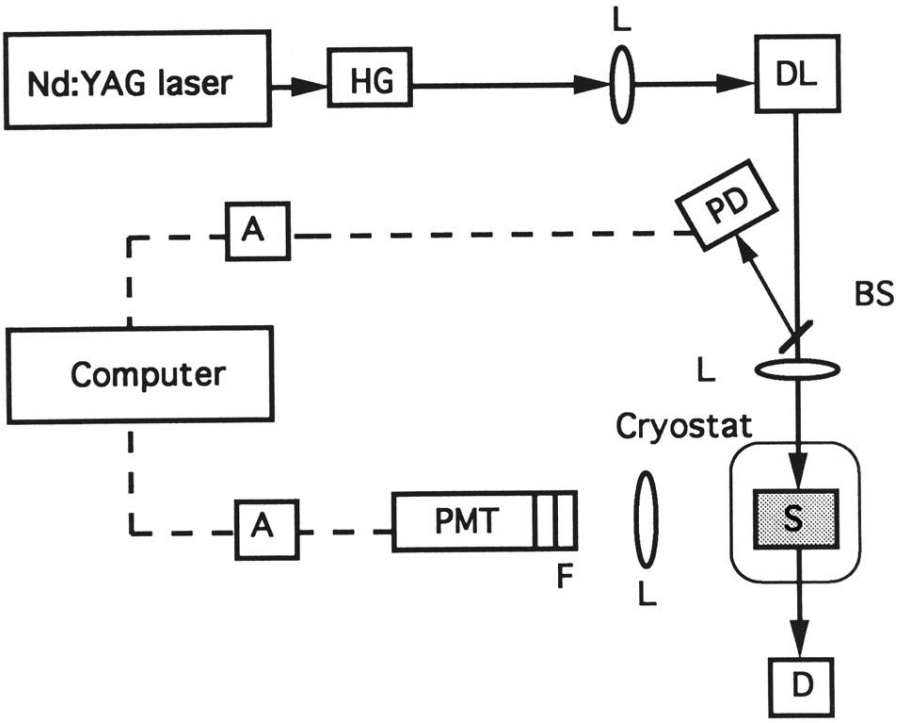

FIG. 4. A schematic diagram of the experimental arrangement used for two-photon excitation measurement. Key: A=gated integrator and boxcar averager, BS=beam splitter, D=beam dump, DL=dye laser, F=filter, HG=harmonic generator, L=lens, PD=photodiode, PMT=photomultiplier tube, S=sample.